Structural changes across thermodynamic maxima in supercooled liquid tellurium: A water-like scenario

Peihao Sun[a,b,1] , Giulio Monaco[b] , Peter Zalden[c] , Klaus Sokolowski-Tinten[d,e] , Jerzy Antonowicz[f] , Ryszard Sobierajski[g] , Yukio Kajihara[h] , Alfred Q. R. Baron[i] , Paul Fuoss[a], Andrew Chihpin Chuang[j], Jun-Sang Park[j], Jonathan Almer[j], and J. B. Hastings[a,1]

Liquid polymorphism is an intriguing phenomenon that has been found in a few single-component systems, the most famous being water. By supercooling liquid Te to more than 130 K below its melting point and performing simultaneous small-angle and wide-angle X-ray scattering measurements, we observe clear maxima in its thermodynamic response functions around 615 K, suggesting the possible existence of liquid polymorphism. A close look at the underlying structural evolution shows the development of intermediate-range order upon cooling, most strongly around the thermodynamic maxima, which we attribute to bond-orientational ordering. The striking similarities between our results and those of water, despite the lack of hydrogen-bonding and tetrahedrality in Te, indicate that water-like anomalies may be a general phenomenon among liquid systems with competing bond- and density-ordering.

thermodynamic anomalies | supercooled liquid | liquid–liquid transition | intermediate-range order | two-state model

Liquid polymorphism, or the existence of two or more liquid phases of the same substance, is a topic of much current interest (1, 2). Although the concept dates back to at least the 1960s (3), supporting evidence had been lacking until recent years, when observations of phenomena related to liquid polymorphism began to emerge in a variety of systems. Perhaps the most intriguing among these are single-component systems, where the polymorphism points out the insufficiency of the theory of simple liquids (4) to describe real, albeit compositionally simple, fluid systems, while suggesting the strong influence of local structures, even for the properties of amorphous materials. The current list of systems with clear experimental evidence for a liquid–liquid transition (LLT), in decreasing complexity, includes large molecules, such as triphenyl phosphite (5), and atomic systems, such as phosphorus (6, 7), sulfur (8), and cerium (9). Meanwhile, an LLT has been suggested in many other systems with varying degrees of experimental and theoretical evidence (2).

Among these systems, water is perhaps the most famous. It is well-known that water exhibits a number of thermodynamic anomalies, such as a density maximum at $4\,°C$ under ambient pressure. Among the different scenarios explaining water's anomalies (10, 11), the second critical-point hypothesis (12) has emerged to be a leading theory, as it is observed in recent simulations of water models (13, 14), while also consistent with experimental results (15, 16) [although the latter ones are not without controversy (17, 18)]. Under this framework, there exists an LLT in water in the deeply supercooled region and under elevated pressures, and the coexistence line of this LLT terminates at a liquid–liquid critical point (LLCP). A peculiar aspect of the LLT in liquid water, distinguishing it from most other systems, is the fact that the low-density liquid phase lies on the low-temperature side of the transition. While this explains the density maximum in a straightforward way (11, 12), it also leads to the distinctive phase diagram, where the LLT exists at higher pressures than the LLCP, thus setting water apart from other single-component systems mentioned above. In addition, the critical pressure is predicted to be positive, but not far from zero, so thermodynamic effects related to critical fluctuations can be observed along the $P \approx 0$ isobar (15). These effects manifest as maxima in thermodynamic response functions, such as the isothermal compressibility, and they form a line emanating from the LLCP usually referred to as the Widom line (19). For ordinary water (H_2O), evidence suggests that the Widom line intersects the $P \approx 0$ isobar around 229 K (15). A schematic phase diagram proposed for water is shown in *SI Appendix*, Fig. S1.

In general, the physical origin of water's peculiarities is not entirely clear, and it remains an open question whether they are unique to water or are general to a family of liquids. In fact, it has been suspected that other tetrahedrally coordinated systems (such as silicon) exhibit similar behaviors (20, 21). Another candidate is liquid tellurium (Te), whose lack of tetrahedrality makes it a somewhat surprising example. As observed first by Kanno et al.

Significance

Liquids are traditionally modeled as disordered systems with a given short-range order. This assumption has been challenged, however, by the observation of anomalous thermodynamic behavior in the most common liquid on earth—water—with accumulating evidence pointing to the possible existence of two liquid forms. Here, by measuring deeply supercooled liquid tellurium with X-ray scattering, we find anomalies that closely resemble those of water. A detailed look into the microscopic structure further reveals the mechanism behind and indicates the importance of bond-ordering for the properties of the liquid. Our results suggest that the physics behind water-like thermodynamic anomalies may be common to a family of liquids.

[1]To whom correspondence may be addressed. Email: peihao.sun@unipd.it or jbh@slac.stanford.edu.

(22) and reiterated by Angell (23), liquid Te also exhibits a variety of thermodynamic anomalies, which bear a striking resemblance to those of water. A systematic study of the properties of liquid Te thus can be informative on the universality of water-type LLT, bearing significance from a fundamental physics aspect. From a practical point of view, Te is the basis element of several phase-change materials (PCMs) that are becoming increasingly important for information technology (24). Thus, it is reasonable to expect that the phenomena attributed to liquid polymorphism in Te-based PCMs (25) are related to a possible LLT in liquid Te.

Therefore, in this work, we study the properties of bulk supercooled liquid Te under low vapor pressure (<0.5 mbar). We observe maxima in various thermodynamic response functions, including the isothermal compressibility, around 615 K. Moreover, we are able to determine details of the structural changes across the thermodynamic response maxima, which show many similarities with those of water. Our results clearly show that intermediate-range ordering plays a central role in the structural modification and indicate that water-like thermodynamic anomalies may be attributed to a competition between density- and bond-ordering, regardless of the details of the local structure.

Simultaneous Small-Angle and Wide-Angle X-Ray Scattering

In order to systematically study the thermodynamic and structural changes, we performed simultaneous small-angle X-ray scattering (SAXS) and wide-angle X-ray scattering (WAXS) measurements at beamline 1-ID at the Advanced Photon Source. The high X-ray photon energy, 76.112 keV, allows us to probe bulk Te samples in a simple transmission geometry (see *Materials and Methods* for details).

Our dataset includes three scans. The scans are temporally separated during the experiment, performed on different samples, and the X-ray beam condition differs between the scans. The consistency of the results from all scans, as will be shown below, strongly supports our conclusions. Each scan consists of several rounds of temperature cycling, where in each round, the sample is first heated above its melting point of 723 K and then cooled down in steps (usually 10 K) to the lowest temperature. At each step, after temperature equilibration, X-ray scattering patterns are collected for several minutes. Recrystallization happens suddenly and can be identified by the appearance of sharp Bragg peaks in the WAXS pattern; these data are excluded from the analysis.

Fig. 1 shows the WAXS and SAXS results from scan 1. The structure factor $S(Q)$ is obtained from the WAXS patterns, and the results agree well with those in the literature (*SI Appendix*). Several trends can be clearly observed. First, with cooling, the first peak moves to lower Q values, which is similar to the behavior of water (15, 26). The second peak becomes sharper, while its position remains relatively constant at $3.3\,\text{Å}^{-1}$. The broad third peak spanning 4 to $6\,\text{Å}^{-1}$ gradually changes its symmetry upon cooling, with the low-Q side centered around $4.4\,\text{Å}^{-1}$ decreasing in magnitude and the high-Q side centered around $5.1\,\text{Å}^{-1}$ growing. Remarkably, the same phenomenon has been observed in ab initio molecular dynamics (AIMD) simulations (27), although the growth of the high-Q side becomes obvious in that study only at the very low temperature of 560 K.

An interesting feature is the presence of a prepeak centered around $1.4\,\text{Å}^{-1}$. More detailed analysis of this prepeak will be presented in *Structural Changes*. We note here that a prepeak is also observed in Te-based chalcogenides, such as $Ge_{15}Te_{85}$ (28–31), as well as PCMs (32), particularly in the supercooled
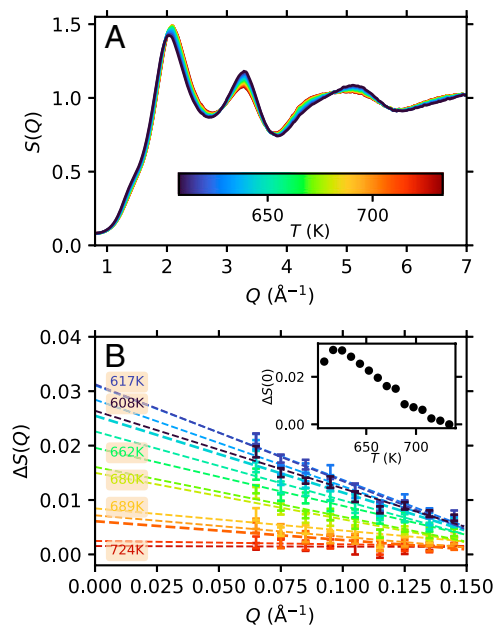

Fig. 1. (*A*) Te WAXS profiles (structure factor $S(Q)$) from scan 1. From dark red to dark blue are decreasing temperatures, as indicated by the color bar. (*B*) Te SAXS profiles from the same scan, subtracting the highest temperature profile (733 K) in the scan. The color scheme is the same as in *A*. Data are shown with error bars, and the dashed lines show linear fits to the data. Several temperatures are marked next to the fit lines with the corresponding colors. *B, Inset* shows the intercept $\Delta S(0)$ plotted against sample temperature; the error bars are smaller than the symbol.

liquid region. In these materials, the appearance of the prepeak is attributed mostly to the Ge atoms (29) and explained as a Peierls-like distortion (30, 31). Here, in pure Te, the prepeak is found to exist above the melting point as well, where the liquid is metallic (33). Therefore, a Peierls-like distortion is unlikely, while it is possible that the prepeak arises from bond-orientational order, as will be discussed later.

For SAXS, as in most other atomic liquids, the structure factor of liquid Te is much less than unity, and the scattering is weak. Consequently, the background is significant, and its pattern depends on the position of the sample and the furnace, and, thus, it is difficult to be measured and subtracted accurately. Nonetheless, within each scan, sample movement is negligible, and the background pattern is expected to remain unchanged. Therefore, for the SAXS analysis, we calculate the change in the structure factor, $\Delta S(Q)$, from the highest temperature in each scan, which cancels out the background. For scan 1, this is 733 K, above the melting point at 723 K. The results are shown in Fig. 1*B*, and they show unambiguously a nonmonotonic behavior with cooling: While $\Delta S(Q)$ increases at first, it begins to decrease at the lowest temperatures. To quantify the change, as in earlier works on chalcogen systems (34), we fit a linear function to $\Delta S(Q)$ with the results shown as dashed lines. The extracted intercept, $\Delta S(0)$, is plotted against temperature in Fig. 1 *B, Inset*, and a peak can be clearly observed. This suggests the existence of thermodynamic maxima, to be discussed below.

Maxima in the Thermodynamic Response Functions

The nonmonotonic behavior in the SAXS region bears much resemblance to recent results on supercooled water (15), where it is found to associate with the LLT. We now look further into the extent of similarities between the two systems. The density maximum at 4 °C is often thought to be a salient anomaly
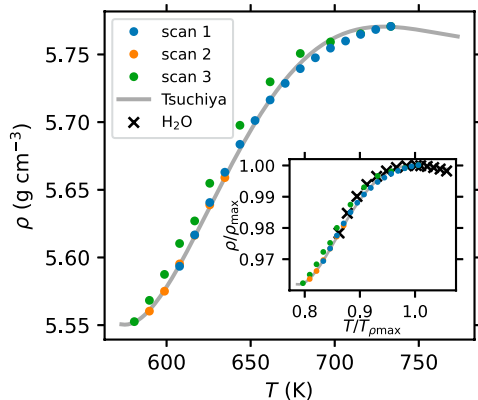
Fig. 2. Density of liquid Te plotted against temperature. Dots with different colors show results from the three different scans, which agree well with each other and with the data reported by Tsuchiya (35) (gray line). *Inset* shows the same data in reduced temperature and density, which are normalized by the location of density maximum $\rho_{max} = 5.77$ g/cm^3 around $T_{\rho max} = 729$ K. Black crosses show the results on supercooled (36) and normal liquid water (37), which bear remarkable resemblance to Te.

of water. Fig. 2 shows our results from all three scans on the density of supercooled liquid Te obtained with X-ray transmission measurements (*SI Appendix*). The results are consistent between scans, and all agree well with the values reported by Tsuchiya (35). Fig. 2, *Inset* shows the same data plotted on reduced scales normalized by the maximum density $\rho_{max} = 5.77$ g/cm^3 and the corresponding temperature $T_{\rho max} = 729$ K. When the available data on water are plotted on the same reduced scale (with $\rho_{max} = 1$ g/cm^3 and $T_{\rho max} = 277$ K), a remarkable resemblance between the two systems can be observed, as has been pointed out in the literature (22, 23). In comparison, other tetrahedral systems, such as silica (in experiment) (38) and silicon (in simulation) (39), show a density maximum that is significantly broader. Thus, the similarities between Te and water may suggest that the degree of structural ordering is comparable between them (40).

As in the case of water (11), the density anomaly in liquid Te hints at the possible existence of liquid polymorphism. To provide further evidence for this scenario, in Fig. 3, we show, with colored symbols representing different scans, four properties of liquid Te: the $Q \to 0$ limit of the structure factor, $S(0)$ (Fig. 3A); the isothermal compressibility, $\kappa_T \equiv -V^{-1}(\partial V/\partial P)_T$ (Fig. 3B); the temperature derivative of the position of the first peak, Q_{m1} (Fig. 3C); and the opposite of the thermal expansion coefficient $\alpha_P \equiv V^{-1}(\partial V/\partial T)_P$ (Fig. 3D). Of these quantities, Q_{m1} can be obtained from the WAXS data in a straightforward way, and α_P can be derived from the density measurement shown above. To obtain $S(0)$ and κ_T, we use the following relation (41):

$$S(0) = k_B T \frac{\rho}{m} \kappa_T, \qquad [1]$$

where k_B is the Boltzmann constant and m is the mass of the Te atom. For $S(0)$, the value at the highest temperature for each scan is determined by using Eq. (1) and a known value of κ_T: For scans 1 and 3, this is above the melting point, and we use the value given in ref. 35; for scan 2, we use the results from the other two scans. Because we have measured the relative change $\Delta S(0)$ from the highest temperature, the values of $S(0)$ and κ_T are then obtained. The presence of maxima is evident in all panels of Fig. 3. For $S(0)$ and κ_T, we note that, although the procedure described above is used to obtain their absolute values, the maxima can already be seen in $\Delta S(0)$, as shown in Fig. 1B, as well as *SI Appendix*, Figs. S10B and S11B. The approximate position of the maxima, 615 K, is marked with a dashed vertical line in Fig. 3,

while the shaded region indicates a ± 10 K range as a guide to the eye.

The existence and the shape of these maxima provide crucial information on the thermodynamics of liquid Te—in particular, the possible morphology of its liquid-phase diagram, which has not been discussed much in the literature. Given the similarities between the thermodynamic properties of Te and water, however, it is reasonable to refer to studies on the latter, of which an extensive amount exist. Specifically, to explain water's thermodynamic anomalies, most of which are shared by Te, four scenarios have been proposed (10, 11): 1) the "retracting spinodal" scenario (42), where the anomalies are consequences of the liquid–vapor spinodal re-entering the supercooled liquid region; 2) the "second critical point" scenario (12), where the anomalies are effects related to an LLCP located in the supercooled region at positive pressures; 3) the "hidden critical point" scenario (43), where the LLCP is located in the unstable region defined by the liquid–vapor spinodal and is thus unreachable; and 4) the "singularity free" scenario, where the thermodynamic maxima exist, but there is no critical point on the phase diagram (44). For liquid Te, the maxima observed in Fig. 3 rule out scenario (1), which predicts divergence due to the spinodal (42), while the breadth of these maxima and the continuous change in the structure factor (e.g., Q_{m1}) excludes scenario (3) where a first-order LLT is expected (43).

Therefore, we are left with the LLCP scenario (2) and the singularity-free scenario (4). The present results do not fully confirm or exclude either case, since the fluctuations observed here are not large enough to be attributed to large-scale critical fluctuations, which only exist very close to a critical point. However, it should be noted that the mechanism underlying the singularity-free models proposed so far is the existence of two local states in the liquid and the interconversion between them, which is often referred to as the "two-state model" (2, 11, 45, 46).
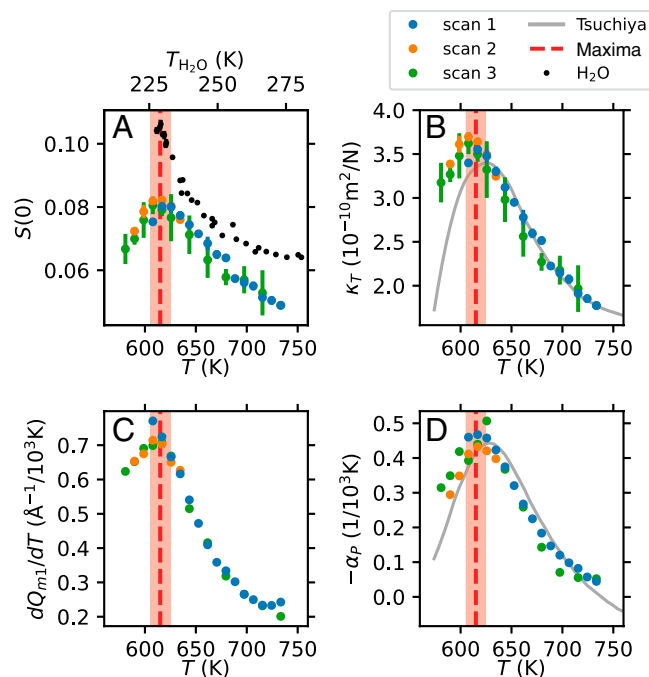
Fig. 3. Maxima in the properties of supercooled Te. $S(0)$ (*A*), isothermal compressibility, κ_T (*B*), temperature derivative of the first peak position, Q_{m1} (*C*), and the opposite of the thermal expansion coefficient α_P (*D*), all plotted against sample temperature T. Results by Tsuchiya (35) are shown as gray lines in *B* and *D*. The vertical dashed line shows the approximate position of the maxima, 615 K, and the red shaded region indicates a ± 10 K range around it as a guide to the eye. In *A*, we also plot $S(0)$ for water (small black dots, upper x axis) (15).

Several of these models can be understood as variations of the LLCP model, where the LLCP is inaccessible, for example, because it is located at $T = 0$ K (44, 47) or because the critical density is too high to be reached (45). In those cases, the physics governing the behavior of the liquid is the same as that for the "supercritical" states in the LLCP scenario, which include the $P = 0$ isobar. Nonetheless, given the lack of an actual LLCP in those cases, it may not be accurate to use the term "Widom line" to describe the thermodynamic response maxima; instead, the term "Schottky line," derived under the framework of the two-state model, has been used in some works (2, 48). Since our results do not distinguish between the two scenarios, in this work, we simply use the phrase "thermodynamic response maxima" to refer to their approximate position, 615 K. It should be mentioned that similar controversies surround the interpretation of results on supercooled water as well (2, 45); perhaps the most convincing proof would be to find the LLCP with critical-like behavior in its vicinity, as has been done in the molecular dynamics simulations of several water models (2, 13).

Notably, the maxima in all quantities shown in Fig. 3 are close to each other in temperature. This is an important observation because different quantities are expected to have a different background contribution given by the behavior of a normal liquid (48). In particular, for ordinary liquids, κ_T increases with temperature, so the peak in κ_T is expected to shift to somewhat higher T; on the other hand, $-\alpha_P$ decreases with temperature for normal liquids, so the peak in $-\alpha_P$ should be shifted to lower T. The fact that the peaks in Fig. 3 B and D are very close in temperature means that the shifts are small; this is also consistent with the sharpness of the peaks. Therefore, 615 K should be a good approximation of the position of the Schottky or Widom line for liquid Te at $P \approx 0$.

Further evidence for the similarity between Te and water can be seen in Fig. 3A, where the measured values of $S(0)$ in supercooled water (15) are also shown. Note that $S(0)$ is a dimensionless quantity reflecting the number fluctuations in the system (41):

$$S(0) = \frac{\langle (N - \langle N \rangle)^2 \rangle}{\langle N \rangle}, \qquad [2]$$

where N is the number of particles (Te atoms or water molecules) in a given sample volume, and the angular brackets denote the ensemble average. Thus, the fact that $S(0)$ is close in magnitude between Te and water at $P \approx 0$ indicates that, if the LLCP exists, the critical pressure in liquid Te may be as close to zero pressure as in water.

Structural Changes

Pertinent to the phenomenon of liquid polymorphism is the underlying structural transformation between the different liquid forms. The WAXS data, with examples given in Fig. 1A, allow us to examine the microscopic structural changes across the thermodynamic maxima in detail. Our experimental setup provides data up to $Q = 7\,\text{Å}^{-1}$, and previous works have shown that little change appears in $S(Q)$ beyond 6 Å^{-1} across a range of 500 K (27, 49). Therefore, we append literature data from 7 to 15 Å^{-1} (27, 50) to our results to obtain the radial distribution function $g(r)$ (further details are in *SI Appendix*), which describes the average density at a distance r from a reference atom. In Fig. 4A, we show the function $r^2 g(r)$ with cooling from 738 K to 585 K. Two salient features emerge: a decrease in the region between ~3 Å and ~3.7 Å and an increase in the broad second peak from 3.7 to 4.7 Å. In Fig. 4B, we plot the running coordination number, $N(r)$, which is obtained from $g(r)$ and represents the averaged number of atoms within a distance r from the reference atom. Indeed, the change in $N(r)$ is small up to $R_1 = 3.14\,\text{Å}^{-1}$, where the data appear to have an isosbestic point. We thus take R_1 to be the boundary of the first coordination shell, resulting in a coordination number of ~2.1 under all temperatures. Remarkably, the position of R_1 also lies close to the first minimum in $g(r)$ of amorphous Te (52), as shown in Fig. 4A, which further supports this choice of R_1 as the boundary of the first shell.

Here, we note that earlier works attributed the structural transition in liquid Te to a decrease of coordination number from three to two upon cooling (33). However, this model has been much debated in the literature (53), and it was pointed out that the measured coordination number depends sensitively on both the exact definition of the first shell boundary (54) and the available
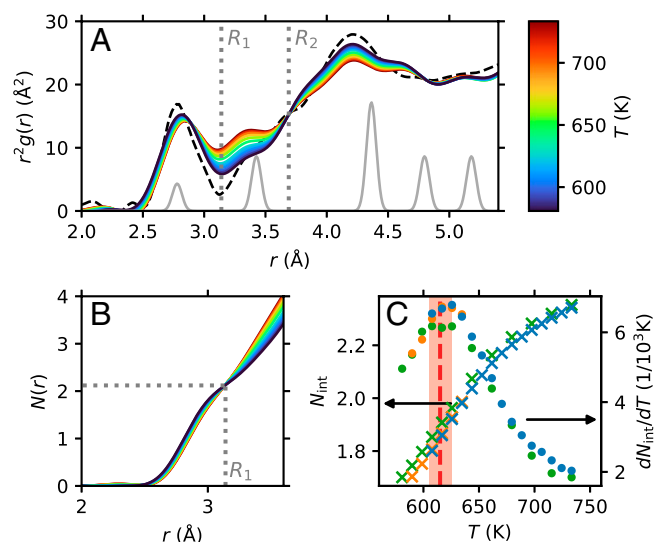
Fig. 4. Temperature evolution of the structure of liquid Te. From dark red to dark blue, the temperature decreases from 738 K to 585 K, as shown in the color bar. *A* shows the function $r^2 g(r)$, and *B* shows the running coordination number $N(r)$. Also shown in *A* are trigonal Te (51) (gray solid line) and electron-diffraction results on amorphous Te (52) (black dashed line). Vertical lines: We take R_1, the isosbestic point in *B*, as the boundary of the first shell; R_2 is a near-isosbestic point in *A* and is taken to be the lower boundary of the second shell. *C* shows the number of atoms in the intermediate region (crosses, left y axis) between R_1 and R_2 for all three scans, as well as its temperature derivative (dots, right y axis). The derivative shows a peak close to the thermodynamic response maxima in Fig. 3 (dashed vertical line).

Q range (55). In fact, more recent AIMD results (27) show that even the trend depends on the cutoff radius of the first shell: If the cutoff is at 3.1 Å, the coordination number increases with cooling, while it decreases with a cutoff at 3.2 Å. Notably, this is consistent with our observation that the coordination number remains constant with a cutoff around 3.14 Å, leading to the conclusion that the coordination number alone does not explain the behavior of supercooled Te.

The plots shown in Fig. 4 *A* and *B* bear a notable resemblance to recent measurements on water (26). In particular, an isosbestic point was also found in the running coordination number $N(r)$ of water, leading to the conclusion that the first shell coordination is mostly constant from 300 K down to 244.2 K (26). In addition, a depletion of molecules was found upon supercooling in the region between the first and second peak, referred to as the interstitial region (26). This means that for both water and Te, intermediate-range ordering, instead of changes in first-shell coordination, drives the structural changes upon cooling and possibly distinguishes the two liquid structures: The high-temperature liquid is dominated by a denser and more disordered structure, including more interstitial atoms, while the low-temperature liquid is dominated by a less dense and more ordered structure up to the second shell.

To quantify the structural changes in liquid Te, we calculate the rate of depletion of atoms in between the first and second peaks, hereinafter referred to as the intermediate region. The lower boundary of this intermediate region is the first shell boundary R_1, while we define the upper cutoff R_2 as the near-isosbestic point observed in $r^2 g(r)$, around 3.69 Å^{-1}. Although this choice of R_2 is somewhat arbitrary, small changes do not alter the conclusions below (*SI Appendix*). We can then obtain the number of atoms between R_1 and R_2, N_{int}, as a function of temperature. The results are plotted as crosses in Fig. 4*C*, and N_{int} increases with temperature, as expected. Further, the temperature derivative of N_{int} can be obtained, as shown in the same panel, and it shows a peak similar in both position and shape to the maxima in Fig. 3. This provides strong evidence that the thermodynamic changes in Fig. 3 are accompanied by a fast depletion of atoms in the intermediate region, signifying an increase in intermediate-range ordering.

The growing intermediate-range order can also be seen in the rise of the prepeak shown in Fig. 1*A*. A closer look reveals that, with cooling, the center of the prepeak moves to lower Q similar to the first peak, Q_{m1}. Therefore, to compare the prepeak at different temperatures, in Fig. 5*A*, we plot the structure factor

as a function of the reduced momentum transfer, Q/Q_{m1}. In order to better visualize the prepeak, we subtract a background indicated by the dotted line. The background is modeled as a 3rd-degree polynomial and fit with data before and after the prepeak, $0.45 < Q/Q_{m1} < 0.55$ and $0.80 < Q/Q_{m1} < 0.90$, where $S(Q/Q_{m1})$ appears to change little with temperature (nevertheless, due to a possible temperature dependence, we specifically choose the data at $T \approx 610$ K for the fit). After background subtraction, the data in the prepeak region, denoted here as $S_{pp}(Q/Q_{m1})$, is shown in Fig. 5 *A, Inset*. Here, the near-Gaussian shape of the prepeak and its growth with cooling become clear. Remarkably, the center position appears to remain the same at all temperatures. This means that the temperature dependence of the Q position of the prepeak follows almost exactly that of the prepeak, suggesting that they may share a common origin in the local structure.

For a more quantitative analysis, we obtain the integrated prepeak intensity, $I_{pp} = \int_{0.55}^{0.80} S_{pp}(q_r) dq_r$, where $q_r \equiv Q/Q_{m1}$. The temperature evolution of I_{pp} is shown in Fig. 5*B*. Below $\sim$690 K, I_{pp} increases with cooling, gaining around 40% toward the lowest temperature measured. The increase with heating above 690 K, on the other hand, may be due to temperature-dependent changes in the background. These changes are difficult to model, and because the prepeak is a small-amplitude feature overlaid on a rapidly rising background, as can be seen in Fig. 5*A*, performing temperature-dependent fitting of the background leads to noisy and model-dependent results. Therefore, we have chosen to subtract the same background for all temperatures. In Fig. 5*C*, we plot the temperature derivative, $-dI_{pp}/dT$, where a peak can be seen close to the position of the thermodynamic response maxima. This signifies a rapid development of intermediate-range order consistent with the observations above. We note that, because a constant background is subtracted from all temperatures, the value of $-dI_{pp}/dT$ is independent from the modeling of this background. However, when interpreting the results, one should bear in mind that the temperature dependence of the actual background may contribute to the values of $-dI_{pp}/dT$; an accurate modeling of this background could be the subject of future work.

Discussion and Conclusions

The results above have shown clear evidence for rapid intermediate-range ordering across the thermodynamic response maxima in supercooled Te, but details of this ordering remain to be discussed. Here, we propose that bond-orientational order plays a crucial
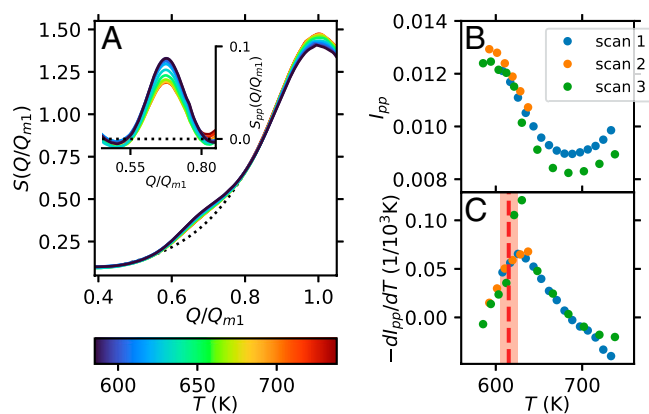
Fig. 5. Analysis of the prepeak. (*A*) The structure factor plotted as a function of reduced momentum transfer, Q/Q_{m1}, focusing on the low-Q region. From dark red to dark blue, the temperature decreases from 738 K to 585 K, as shown in the color bar. The dotted line shows the estimated background (see *Structural Changes*). *A, Inset* shows the prepeak region with the background subtracted. (*B* and *C*) The integrated prepeak intensity, I_{pp} (*B*) and the negative of its temperature derivative (*C*), both plotted as function of temperature. The derivative shows a peak close to the thermodynamic response maxima in Fig. 3 (dashed vertical line).

role. The prepeak, centered around $Q_{pp} = 1.4 \, \text{Å}^{-1}$, signals the presence of some structure on the order of $2\pi/Q_{pp} = 4.5 \, \text{Å}$. In the crystal, this corresponds to the distance between next-nearest neighbors within a chain (i.e., the third peak of trigonal Te in Fig. 4A), whose bonds with their common neighbor form an angle of $103.2°$ (51). The second peak in the liquid $g(r)$ is also close to 4.5 Å, but slightly lower in r, indicating a somewhat smaller average bond angle, consistent with AIMD results (27). With decreasing temperatures, the prepeak grows as discussed above, while AIMD shows that the bond-angle distribution becomes sharply peaked around 96° (27). In addition, the AIMD results have shown that two-coordinated atoms (within a soft cutoff around 3.2 Å) have a bond-angle distribution, which is strongly peaked around 100°, whereas atoms with higher coordination show a broader bond-angle distribution peaked close to 90° (27). This suggests that an increase in bond-orientational order would lead to a decrease in atoms in the intermediate region, as we have observed.

The similarities between Te and water in the various aspects we have discussed are worth emphasizing for several reasons. Firstly, the thermodynamic similarities indicate that the liquid-phase diagrams of Te and water are likely similar. Thus, investigations into one may provide vital information for the other. Secondly, the similarities between the structural evolution of the two suggest a common microscopic origin. Our results confirm that a reduction in atoms in the intermediate region between the first and second peaks in $g(r)$, similar to the depletion of interstitial atoms observed in water (26), indeed accompanies the transition across the thermodynamic response maxima in liquid Te; such data are not yet available in water due to difficulties in reaching the deep supercooled state. Last, but not least, the observed similarities strongly indicate that the anomalies of water are not limited to systems with hydrogen-bonding or tetrahedral coordination, as is usually thought, but are general to a family of liquids. Finding the common features between Te and water may thus help generalize the origin of the observed phenomena. For example, it is well-known that water and other tetrahedral systems have an "open" local structure, while AIMD results have revealed an unusually large volume fraction of "cavities" in liquid Te as well (27). On the other hand, the number of bonds is rather different between Te (two or three per atom) and water (four or five per molecule), and, thus, our observations indicate that the degree of thermodynamic anomalies cannot be predicted by bond-number fluctuations alone.

Finally, we note that the enhanced intermediate-range ordering in the low-temperature limit is consistent with the two-state model mentioned above (2, 46), where the thermodynamic anomalies (such as the density maximum) are caused by an increasing amount of locally favored, albeit less dense, structures upon cooling. Since the presence of locally favored structures is expected in a number of liquids (2), it is reasonable to predict that more systems can be found to exhibit water-type anomalies.

Studying the commonalities and differences between these systems may help reveal the role of intermediate-range structures and bond-orientational ordering in the behavior of liquids in general.

In conclusion, using a combination of SAXS and WAXS, we have observed clear maxima in the thermodynamic response functions in supercooled liquid Te, as well as the structural changes that accompany it. Our results suggest that intermediate-range ordering, likely of a bond-orientational nature, is strongly associated with the anomalous properties of liquid Te. This is consistent with the two-state model and points to the possibility of liquid polymorphism in this system. Moreover, the striking resemblance between Te and water in various properties, despite their different local structures, points to the possible existence of water-like thermodynamic anomalies in a family of liquid systems. Thus, our study suggests that the competition between bond- and density-ordering can be a general phenomenon and plays a crucial role in the thermodynamics of liquid systems.

Materials and Methods

The samples used in this study are Te powder (99.999% metals basis; purchased from Alfa Aesar) vacuum-sealed in borosilicate glass ampoules. The inner diameter of the glass container is around 0.7 mm, and its wall thickness is around 0.085 mm.

The experiment was performed at beamline 1-ID at the Advanced Photon Source. The X-ray energy was 76.112 keV. The planes of the WAXS and SAXS detectors are 2.003 m and 6.420 m from the sample, respectively. The Q positions of the WAXS detector pixels were calibrated by using a CeO_2 powder sample.

Further details on the experimental setup are provided in *SI Appendix*.

Data Availability. All study data are included in the article and/or *SI Appendix*. Numerical data is also available in Zenodo (56).

Author affiliations: ªSLAC National Accelerator Laboratory, Menlo Park, CA 94025; ᵇDipartimento di Fisica e Astronomia "Galileo Galilei," Università degli Studi di Padova, 35131 Padova, Italy; ᶜEuropean XFEL, 22869 Schenefeld, Germany; ᵈFaculty of Physics, University of Duisburg-Essen, 47048 Duisburg, Germany; ᵉCenter for Nanointegration Duisburg-Essen, University of Duisburg-Essen, 47048 Duisburg, Germany; ᶠFaculty of Physics, Warsaw University of Technology, Warsaw 00-662, Poland; ᵍInstitute of Physics of the Polish Academy of Sciences, PL-02-668 Warsaw, Poland ʰGraduate School of Advanced Science and Engineering, Hiroshima University, Higashi-Hiroshima 739-8521, Japan; ⁱMaterials Dynamics Laboratory, RIKEN SPring-8 Center, Sayo 679-5148, Japan; and ʲX-Ray Science Division, Advanced Photon Source, Argonne National Laboratory, Lemont, IL 60439

1. H. E. Stanley, Ed., *Liquid Polymorphism* (Advances in Chemical Physics, John Wiley & Sons, Inc., Hoboken, NJ, 2013), vol. 152.
2. H. Tanaka, Liquid-liquid transition and polyamorphism. *J. Chem. Phys.* **153**, 130901 (2020).
3. E. Rapoport, Model for melting-curve maxima at high pressure. *J. Chem. Phys.* **46**, 2891–2895 (1967).
4. J. P. Hansen, I. R. McDonald, *Theory of Simple Liquids* (Academic Press, London, ed. 3, 2006).
5. R. Kurita, H. Tanaka, Critical-like phenomena associated with liquid-liquid transition in a molecular liquid. *Science* **306**, 845–848 (2004).
6. Y. Katayama et al., A first-order liquid-liquid phase transition in phosphorus. *Nature* **403**, 170–173 (2000).
7. G. Monaco, S. Falconi, W. A. Crichton, M. Mezouar, Nature of the first-order phase transition in fluid phosphorus at high temperature and pressure. *Phys. Rev. Lett.* **90**, 255701 (2003).
8. L. Henry et al., Liquid-liquid transition and critical point in sulfur. *Nature* **584**, 382–386 (2020).
9. A. Cadien et al., First-order liquid-liquid phase transition in cerium. *Phys. Rev. Lett.* **110**, 125503 (2013).
10. G. Pallares et al., Anomalies in bulk supercooled water at negative pressure. *Proc. Natl. Acad. Sci. U.S.A.* **111**, 7936–7941 (2014).
11. P. Gallo et al., Water: A tale of two liquids. *Chem. Rev.* **116**, 7463–7500 (2016).
12. P. H. Poole, F. Sciortino, U. Essmann, H. E. Stanley, Phase behaviour of metastable water. *Nature* **360**, 324–328 (1992).
13. P. G. Debenedetti, F. Sciortino, G. H. Zerze, Second critical point in two realistic models of water. *Science* **369**, 289–292 (2020).
14. J. C. Palmer, P. H. Poole, F. Sciortino, P. G. Debenedetti, Advances in computational studies of the liquid-liquid transition in water and water-like models. *Chem. Rev.* **118**, 9129–9151 (2018).
15. K. H. Kim et al., Maxima in the thermodynamic response and correlation functions of deeply supercooled water. *Science* **358**, 1589–1593 (2017).

16. K. H. Kim et al., Experimental observation of the liquid-liquid transition in bulk supercooled water under pressure. *Science* **370**, 978–982 (2020).

17. F. Caupin et al., Comment on "Maxima in the thermodynamic response and correlation functions of deeply supercooled water". *Science* **360**, eaat1634 (2018).

18. K. H. Kim et al., Response to Comment on "Maxima in the thermodynamic response and correlation functions of deeply supercooled water". *Science* **360**, eaat1729 (2018).

19. L. Xu et al., Relation between the Widom line and the dynamic crossover in systems with a liquid-liquid phase transition. *Proc. Natl. Acad. Sci. U.S.A.* **102**, 16558–16562 (2005).

20. V. V. Vasisht, S. Saw, S. Sastry, Liquid–liquid critical point in supercooled silicon. *Nat. Phys.* **7**, 549–553 (2011).

21. M. Beye, F. Sorgenfrei, W. F. Schlotter, W. Wurth, A. Föhlisch, The liquid-liquid phase transition in silicon revealed by snapshots of valence electrons. *Proc. Natl. Acad. Sci. U.S.A.* **107**, 16772–16776 (2010).

22. H. Kanno, H. Yokoyama, Y. Yoshimura, A new interpretation of anomalous properties of water based on Stillinger's postulate. *J. Phys. Chem. B* **105**, 2019–2026 (2001).

23. A. Angell, Thermodynamics: Highs and lows in the density of water. *Nat. Nanotechnol.* **2**, 396–398 (2007).

24. H. S. P. Wong et al., Phase change memory. *Proc. IEEE* **98**, 2201–2227 (2010).

25. P. Lucas, S. Wei, C. A. Angell, Liquid-liquid phase transitions in glass-forming systems and their implications for memory technology. *Int. J. Appl. Glass Sci.* **11**, 236–244 (2020).

26. C. Benmore, L. C. Gallington, E. Soignard, Intermediate range order in supercooled water. *Mol. Phys.* **117**, 2470–2476 (2019).

27. J. Akola, R. O. Jones, S. Kohara, T. Usuki, E. Bychkov, Density variations in liquid tellurium: Roles of rings, chains, and cavities. *Phys. Rev. B Condens. Matter Mater. Phys.* **81**, 094202 (2010).

28. C. Bergman, C. Bichara, J. P. Gaspard, Y. Tsuchiya, Experimental investigation of the waterlike density anomaly in the liquid $Ge_{15}Te_{85}$ eutectic alloy. *Phys. Rev. B Condens. Matter Mater. Phys.* **67**, 104202 (2003).

29. J. Kalikka, J. Akola, R. O. Jones, S. Kohara, T. Usuki, Amorphous $Ge_{15}Te_{85}$: Density functional, high-energy x-ray and neutron diffraction study. *J. Phys. Condens. Matter* **24**, 015802 (2012).

30. S. Wei et al., Structural evolution on medium-range-order during the fragile-strong transition in $Ge_{15}Te_{85}$. *Acta Mater.* **129**, 259–267 (2017).

31. J. P. Gaspard, Structure of covalently bonded materials: From the Peierls distortion to phase-change materials. *C. R. Phys.* **17**, 389–405 (2016).

32. P. Zalden et al., Femtosecond x-ray diffraction reveals a liquid-liquid phase transition in phase-change materials. *Science* **364**, 1062–1067 (2019).

33. B. Cabane, J. Friedel, Local order in liquid tellurium. *J. Phys. (Paris)* **32**, 73–84 (1971).

34. Y. Kajihara, M. Inui, K. Matsuda, T. Nagao, K. Ohara, Density fluctuations at the continuous liquid-liquid phase transition in chalcogen systems. *Phys. Rev. B Condens. Matter Mater. Phys.* **86**, 214202 (2012).

35. Y. Tsuchiya, Thermodynamic evidence for a structural transition of liquid Te in the supercooled region. *J. Phys. Condens. Matter* **3**, 3163–3172 (1991).

36. R. J. Speedy, Thermodynamic properties of supercooled water at 1 atm. *J. Phys. Chem.* **91**, 3354–3358 (1987).

37. W. Wagner, A. Pruß, The IAPWS Formulation 1995 for the thermodynamic properties of ordinary water substance for general and scientific use. *J. Phys. Chem. Ref. Data* **31**, 387–535 (2002).

38. C. A. Angell, H. Kanno, Density maxima in high-pressure supercooled water and liquid silicon dioxide. *Science* **193**, 1121–1122 (1976).

39. C. Angell, S. Borick, M. Grabow, Glass transitions and first order liquid-metal-to-semiconductor transitions in 4-5-6 covalent systems. *J. Non-Cryst. Solids* **205-207**, 463–471 (1996).

40. R. Shi, H. Tanaka, Impact of local symmetry breaking on the physical properties of tetrahedral liquids. *Proc. Natl. Acad. Sci. U.S.A.* **115**, 1980–1985 (2018).

41. L. A. Feigin, D. I. Svergun, *Structure Analysis by Small-Angle X-Ray and Neutron Scattering*, G. W. Taylor, Ed. (Springer US, Boston, 1987).

42. R. J. Speedy, Stability-limit conjecture. An interpretation of the properties of water. *J. Phys. Chem.* **86**, 982–991 (1982).

43. P. H. Poole, F. Sciortino, T. Grande, H. E. Stanley, C. A. Angell, Effect of hydrogen bonds on the thermodynamic behavior of liquid water. *Phys. Rev. Lett.* **73**, 1632–1635 (1994).

44. S. Sastry, P. G. Debenedetti, F. Sciortino, H. E. Stanley, Singularity-free interpretation of the thermodynamics of supercooled water. *Phys. Rev. E Stat. Phys. Plasmas Fluids Relat. Interdiscip. Topics* **53**, 6144–6154 (1996).

45. F. Caupin, M. A. Anisimov, Minimal microscopic model for liquid polyamorphism and waterlike anomalies. *Phys. Rev. Lett.* **127**, 185701 (2021).

46. H. Tanaka, Bond orientational order in liquids: Towards a unified description of water-like anomalies, liquid-liquid transition, glass transition, and crystallization: Bond orientational order in liquids. *Eur. Phys. J. E* **35**, 113 (2012).

47. K. Stokely, M. G. Mazza, H. E. Stanley, G. Franzese, Effect of hydrogen bond cooperativity on the behavior of water. *Proc. Natl. Acad. Sci. U.S.A.* **107**, 1301–1306 (2010).

48. R. Shi, H. Tanaka, The anomalies and criticality of liquid water. *Proc. Natl. Acad. Sci. U.S.A.* **117**, 26591–26599 (2020).

49. H. Endo, K. Maruyama, H. Hoshino, H. Ikemoto, Local structure of liquid Te studied by neutron diffraction and EXAFS. *Z. Phys. Chem.* **217**, 863–878 (2003).

50. A. Menelle, R. Bellissent, A. M. Flank, A neutron scattering study of supercooled liquid tellurium. *Europhys. Lett.* **4**, 705–708 (1987).

51. C. Adenis, V. Langer, O. Lindqvist, Reinvestigation of the structure of tellurium. *Acta Crystallogr. C* **45**, 941–942 (1989).

52. T. Ichikawa, Electron diffraction study of the local atomic arrangement in amorphous tellurium films. *Phys. Status Solidi* **56**, 707–715 (1973).

53. T. Tsuzuki, M. Yao, H. Endo, Static and dynamic structures of liquid tellurium. *J. Phys. Soc. Jpn.* **64**, 485–503 (1995).

54. A. Menelle, R. Bellissent, A. M. Flank, Short range order in liquid Se-Te system by neutron scattering. *Phys. B: Phys. Condens. Matter* **156-157**, 174–176 (1989).

55. W. Hoyer, H. Neumann, M. Wobst, Structure investigation on liquid tellurium by X-ray and neutron scattering. *Z. Naturforsch. A* **47**, 833–840 (1992).

56. P. Sun, Structural changes across thermodynamic maxima in supercooled liquid tellurium: a water-like scenario. Zenodo. https://doi.org/10.5281/zenodo.6652291. Deposited 16 June 2022.